Optimum Combining for Rapidly Fading Channels in Ad Hoc Networks

Sonia Furman, David E. Hammers, and Mario Gerla
Electrical Engineering and Computer Science Departments, University of California, Los Angeles
Los Angeles, California 90024, U.S.A.

ABSTRACT

Research and technology in wireless communication systems such as radar and cellular networks have successfully implemented alternative design approaches that utilize antenna array techniques such as optimum combining, to mitigate the degradation effects of multipath in rapid fading channels. In ad hoc networks, these methods have not yet been exploited primarily due to the complexity inherent in the network's architecture. With the high demand for improved signal link quality, devices configured with omnidirectional antennas can no longer meet the growing need for link quality and spectrum efficiency. This study takes an empirical approach to determine an optimum combining antenna array based on 3 variants of interelement spacing. For rapid fading channels, the simulation results show that the performance in the network of devices retrofitted with our antenna arrays consistently exceeded those with an omnidirectional antenna. Further, with the optimum combiner, the performance increased by over 60% compared to that of an omnidirectional antenna in a rapid fading channel.

Keywords: Ad hoc networks, fading, multipath, antenna arrays, spatial diversity, optimum combining.

1. INTRODUCTION

Unlike cellular and radar communication systems, ad hoc networks are local area networks (LANs) that communicate over a medium with no observable boundaries, are formed without pre-planning, and exist only for as long as they are needed [1]. The ubiquitous attributes of ad hoc networks provide a powerful combination of both mobile access and configuration flexibility. This enables fast deployment, critical for military applications, recovery operations as well as for opportunities to increase productivity and organizational efficiency. Interestingly, the same inherent features that make these networks so attractive are those that create an additional dimension of complexity, and present a great challenge in the design of the network's protocols and their connectivity elements at the Physical layer.

The transceiver at the Physical layer of the network must have the capability to meet the growing demands for signal robustness in wireless channels that is subject to co-channel interference and multipath fading. Though solutions to enhance link quality by antenna arrays and optimum combining methods have been employed in other wireless communication systems, this approach has not thoroughly been exploited in ad hoc networks and is still in its infancy stages. Until recently, physical size combined with functionality created a barrier to implementations of antenna arrays at the transceiver. State-of-the-art technologies that utilize advanced digital signal processing techniques combined with patch antennas similar to those described in [2], provide cost effective implementations of beamforming-arrays that may be retrofitted to devices configured to operate in ad hoc networks.

Prior related work suggests that there are substantial performance improvements in throughput and packet delay to be gained by employing directional antennas in ad hoc networks. These observations for the most part had been a result of research on enhanced Medium Access Control (MAC) protocols that provide additional attributes to accommodate beamsteering routines for systems that accommodate multiple antennas, at both the transmitter and receiver [3][4]. Further, it has been suggested that the primary contributors to limiting capacity in ad hoc networks is embedded in the nature of transmission from an omnidirectional antenna, and that with directional communications both spatial reuse and range are enhanced [5]. Thus, the baseline benefits acquired due to protocol modifications in the MAC layer to accommodate antenna arrays (directional antennas) in ad hoc network have been quantified and affirmed.

The emphasis in this study differs considerably from former studies on directional antennas in ad hoc networks where the focus was on modified MAC protocols. In contrast to prior work, this work focuses on the design of an optimum combining antenna array that results in increased signal–to-noise-ratio (SNR) at the receiver. To achieve this, we designed accurate antenna patterns for use in the simulation rather than rely on hypothetical models such as those used in prior studies [3][4][5] Further, the simulation performed here is supported by existing MAC protocols implemented in QualNet [6].

Till recently, researches resorted to the analysis of adaptive arrays and spatial diversity methods to establish deterministic models to maximize the SNR at the receiver. This was in part due to limitations in advanced network simulators that did not have means to interpret antenna patterns. With the advent of the QualNet [6] simulator, such limitations no longer prevail. QualNet, which is an advanced research tool, provides vast libraries capable of accommodating network models and their dynamics, as well as options for beamsteering with accurate antenna models. In this work, we used QualNet to empirically determine an optimum combining array based on our design of an 8-element equally spaced linear array. We examined the throughput performance of the network while using radiation patterns with 3 variants of interelement spacing, and determined that the array in a rapid fading channel significantly increased performance compared to that of an omnidirectional antenna.

The remainder of this paper is organized as follows: Section 2 describes our simulation for fading and channel impairments. Section 3 presents the design of an 8-element linear array model used in the network simulation to determine the optimum combining configuration. Section 4 discusses the implications of the 3 variants of interelement spacing on the receiver model. Section 5 describes the ad hoc network environment used in the simulation and the results obtained, followed by a summary and conclusion of the study in Section 6.

2. FADING CHANNELS

The mobile radio channel deviates considerably from the stationary additive white Gaussian noise (AWGN) channel due to continuous variations in the environment, motion of surrounding objects, and the mobility of the device itself. In such an environment, the transmitted signal does not assume to have a line of sight, but instead arrives at the receiver from different paths (multipath) caused by its wave scattering off of building and objects, which results in delays of the multipath signal prior to being combined at the receiver. This phenomenon is known as fading. Fading is a term often used in wireless communication to describe the fluctuation in the amplitude and phase of a radio signal over a time period, or travel distance, and can cause significant degradation in the throughput performance of the network.

Fading channels may be characterized in either the frequency or the time domain. In the frequency domain, we use spectra relationships (bandwidth comparisons) to categorize the fading. Two basic types of fading may be defined on this basis: frequency selective fading where the signal bandwidth (BWs) is greater or equal to the channel coherence bandwidth (BW_c), i.e. BWs >= BW_c and non-frequency selective fading where BWs < BW_c also known as flat fading. In flat fading the variation in amplitude of the multipath signals arriving at the receiver is expressed statistically in terms of a Rayleigh probability distribution function (pdf) Eq. (1). In these channels, the spectrum of the transmitted signal is the same as the spectrum of the received signal. Flat fading results in deep fades and may require up to 20 to 30dB more transmitter power to acquire the equivalent bit error rate (BER) performance of that obtained in an AWGN channel. To meet the increased demand of signal-to-noise ratio (SNR) that will produce acceptable BERs, increasing the transmitter power is not a viable solution. This approach is not only costly but will also produce high levels of co-channel interference. In addition, limitations imposed by the Federal Communications Commission (FCC) on the transmitter's power of 802.11[1] products bound the SNR at the receiver. Subject to these restrictions, in this study we propose solutions with an optimum combining array that will meet the SNR requirements to produce acceptable BERs.

Thus far, we discussed the frequency domain. In the time domain, the measure of coherent time T_c (which is the reciprocal rate of the channel's impulse response) is used to describe the characteristics of the fading. The rate of change of the signal is compared to the rate of change of the channel due to mobility and the Doppler effect (shift). For rapid fading channels, the impulse response changes rapidly within the symbol duration and causes frequency dispersion (also known as Doppler spreading), which leads to signal distortion and is considered only when the rate of change of the channel is due to motion [7]. The implication of this is that when there is relative motion between the transmitter and receiver as in mobile ad hoc networks, the Doppler effect is present in the received signal spectrum, which results in frequency dispersion. If the Doppler spread is much greater than the BW of the transmitted signal, the received signal exhibits rapid (fast) fading. In conditions related to our model, where the transmitted signal (baseband signal of 2Mbps) has a narrower bandwidth than that of the channel (22MHz), large signal fluctuations occur at the receiver due to phase shifts and amplitude variations of the multipath components as evident in Figure 1. The figure illustrates the envelope of the amplitude variations as function of time in a rapid fading channel where 5 multipaths have been used to simulate the effects of fading with and without mobility (v = 10 m/s and v = 0 m/s respectively). The carrier frequency used in the simulation of the fading was 2.4 GHz. The path amplitudes

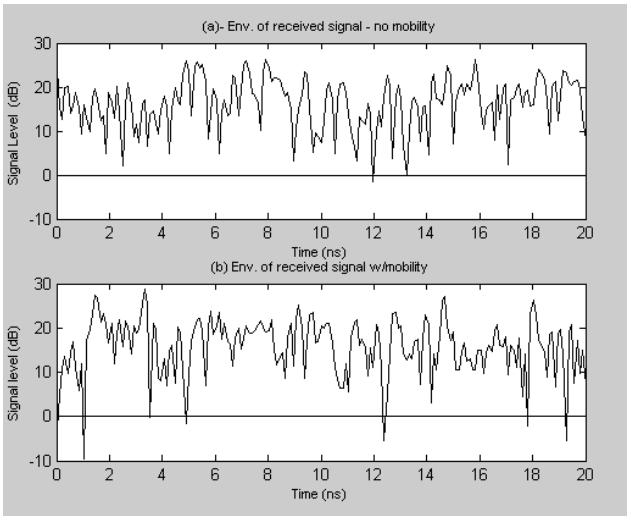

Figure 1 Signal envelope variations in rapid fading channels. (a) no mobility (b) mobility

were generated using a Rayleigh probability distribution function (pdf), Eq. (1) where σ is the rms value of the received voltage signal before envelope detection, and σ^2 is the time average power of the received signal before envelope detection.

$$p(r) = \frac{r}{\sigma^2} e^{-\frac{r^2}{2\sigma^2}} \quad \text{where} \quad 0 \le r \le \infty \qquad (1)$$

To express the phase variations we used the uniform (continuous) distribution that has a constant pdf between its two minimum and maximum parameters, and is appropriate for representing the distribution of round-off errors in values tabulated to a particular number of decimal places [8]. I.e. the random variables assume all its values with equal probability Eq. (2) [9].

$$f(x;k) = \frac{1}{k} \quad \text{for} \quad x = x_1, x_2, \ldots, x_k . \qquad (2)$$

The varying path lengths and phases of the multipath are random, and as result of this, the received power too is a random variable. The 0dB baseline in Figure 1(b) shows that with mobility the signal strength of the envelope of the received signal has deep fades that may dip as low as –10dB, which is significantly below the threshold when compared with the no-mobility case in Figure 1(a). Assuming DQPSK modulation, the envelope of the received signal in Figure 1 is expressed in Eq. (3) as the sum of the 2-quadrature Gaussian components, inphase (I) and quadraphase (Q) of the received signal. With the Doppler effect the received signal is no longer $s(t) = \sum_{i=1}^{N} A_i \cos(\omega_c t + \theta_i)$ but instead becomes Eq. (4), which may be readily expressed in terms of the I and Q .

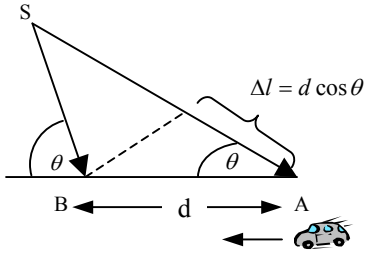

Figure 2. Doppler for mobile traveling from A to B

$$E_{nv} = \sqrt{[I(t)]^2 + [Q(t)]^2} \tag{3}$$

$$s(t) = \sum_{i=1}^{N} A_i \cos(\omega_c t + \omega_d t + \phi_i) \tag{4}$$

where: A_i and ϕ_i are the amplitude and phase of path i respectively; $\omega_c = 2\pi f_c$ - the radian frequency of the carrier; $\omega_d = 2\pi f_d$ - the radian frequency of the Doppler effect, and N is the number of paths (N=5).

Both the carrier frequency f_c and the Doppler frequency were used to represent the spectrum f of the signal in terms of $f = f_c + f_d$, f_d is the Doppler frequency expressed in Eq. (5).

$$f_d = \frac{1}{2\pi}\frac{\Delta\phi}{\Delta t} = \frac{v}{\lambda}\cos\theta \tag{5}$$

where: v is the speed of the mobile and λ the wavelength.

The angle θ in Eq. (5) is a function of the difference in path length, as a result of the mobile traveling a distance d from point A to point B (Figure 2.), assuming the mobile is moving in the direction, towards the wave. The Doppler spread has a significant effect on the spatial channel model due to the correlation observed between pairs of elements in the array. The received signal vector correlation matrix, which specifies these quantities, determines the performance of linear combining arrays. In general for deterministic analysis of array performance the channel model may be developed to provide the spatial correlation function, while for simulation purposes spatial channel model is derived empirically to determine performance through simulation. [10].

3. THE ARRAY MODEL

We designed an 8-element linear antenna array assuming isotropic elements, uniformly excited (UE), and equally spaced with 3 interelement spacing variants to determine the ramifications of the array aperture (and gain) on the throughput performance in an ad hoc network environment, for both an AWGN and a fading channel. Figure 3 illustrates a UE equally spaced linear array (ESLA) that shows the direction of an impinged plane wave originating from an ith source from the direction (θ_i, ϕ_i) where θ_i is the elevation angle and ϕ_i the azimuthal angle. As may be seen in Figure 3, the impinged wave will travel an additional distance Δd before arriving at element m, relative to the element at the origin Eq. (6)

$$(m-1)\Delta d = c\tau_m \tag{6}$$

where: $\Delta d = d\cos\phi_i \sin\theta_i$ (d is the distance between the elements, and c the speed of light, c =3x10^8 m/s).

Assuming the elevation angle θ_i is equal to $\pi/2$, the delay then at element m is τ_m Eq. (7), and the signal received at antenna element m is Eq. (8).

$$\tau_m(\phi_i) = \frac{d}{c}(m-1)\cos\phi_i \tag{7}$$

$$x_m(t) = As(t)e^{-j\beta m\Delta d} = As(t)e^{-j\beta md\cos\phi\sin\theta} \tag{8}$$

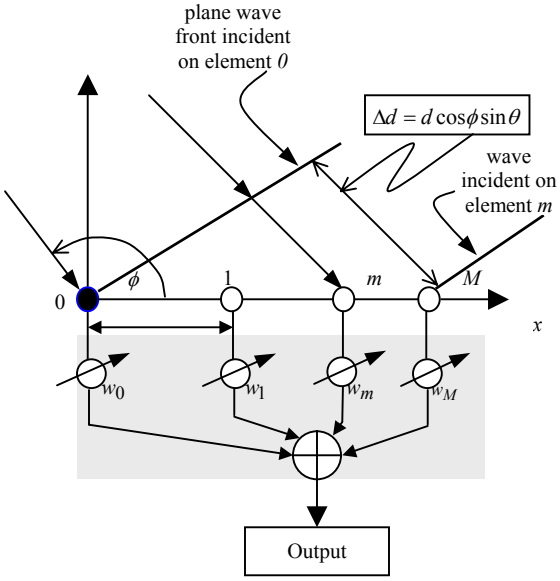

Figure 3 Linear array - UE ESLA

where: A is an arbitrary gain constant; s(t)is the baseband complex envelope representing the modulation of the plane wave; β is the phase propagation factor $2\pi/\lambda$.

The output z(t) of the array is then Eq. (9) or Eq. (10) [10].

$$z(t) = \sum_{m=0}^{M+1} w_m x_m(t) = As(t)\sum_{m=0}^{M+1} w_m e^{-j\beta md\cos\phi\sin\theta} = As(t)f(\theta,\phi) \tag{9}$$

where: $f(\theta,\phi)$ is the array factor and the weighting element w_m associated with the mth branch of the array is $w_m = e^{j\beta md\cos\phi_0}$. By adjusting the set of weights w_m, it is possible to direct the boresight (the direction of maximum radiated power in the main beam), of the array factor in any desired direction of θ,ϕ. In our model, we assume the element patterns $g(\theta,\phi)$ to be identical for each of the elements. For convenience, Eq. (9) is represented in vector form in Eq. (10).

$$\mathbf{z} = \mathbf{w}^H\mathbf{x} \tag{10}$$

where: $\mathbf{x} = [x_1, x_2, ..., x_M]$, $\mathbf{w}^H = ([w_0, w_1, \ldots, w_M]^T)^*$, and H, the Hermitian operator is the conjugate (*) of the transpose vector w^T.

The total field pattern of the array is then the product of the array factor by the element pattern Eq. (11) also known as the pattern multiplication principle. This principle in essence states that a beam or pattern *F(θ,φ)* can be generated by multiplying an element pattern *g(θ,φ)* by its array factor *f(θ,φ)*. The important outcome of this principle is in recognizing that the beams generated are independent of the antenna elements used to form the array [12]. With the assumption that all the elements are similar in the model, the geometry of the antenna, its current distribution, mutual coupling effects, and other electrical characteristics of the elements do not need to be considered in order to produce the radiation patterns. The general normalized power pattern is expressed in Eq. (12).

$$F(\theta,\phi) = g(\theta,\phi)f(\theta,\phi) \tag{11}$$

$$P(\theta,\phi) = |F(\theta,\phi)|^2 \tag{12}$$

An example of a 6-element UE ESLA with an interelement spacing of d= 0.5λ is presented in Figure 4. The radiation pattern constitutes 2 beams, which are 180° apart. In our model, we assume a ground backplane associated with the array to eliminate the second 180° phase shift beam in order to derive at the actual radiation patterns used in our simulation.

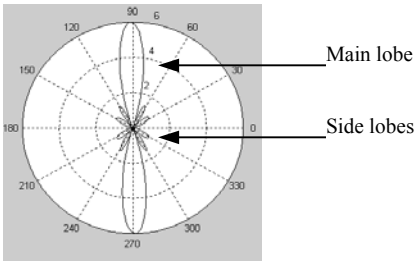

Figure 4 Radiation pattern of a 6-element linear array

The radiation patterns designed for this study are based on an 8-element UE ELSA for $d1 = 0.5\lambda$, $d2 = 1\lambda$, and $d3 = 1.5\lambda$ which represents the 3 interelement spacing variants.

4. THE RECEIVER MODEL

To maximize the SNR at the receiver, we consider 2 approaches (configurations) for the optimum design of the array as a function of interelement spacing. Figure 5 represents both configurations. The first configuration should be viewed as that of an adaptive array. A key issue for adaptive arrays in wireless communications is their performance in multipath verses a line of sight environment. Typically, an adaptive array (or special case, fixed beam array) uses a fraction of a wavelength interelement spacing (e.g. 0.5λ) between elements to avoid grating lobes. The adaptive array implementation in Figure 5 includes a 'Weight adjustment' (*shaded broken-line box*) that relies on various algorithms [12] to dynamically adjust the weights w_m associated with each branch of the array. A special case of the Figure 5 is that with the 'Weight adjustment' (box) removed. In this case, we consider the weights w_m assigned to each of the branches to be predetermined and fixed.

The second configuration that may be construed from Figure 5 is that of 'combining methods' in antenna diversity'. Antenna diversity (or spatial diversity) is described by [13] as multiple antennas spaced sufficiently far apart to achieve decorrelation at the receiver, where the received signal undergoes independent fading processing at each antenna element. For the variants of interelement spacing $d2 = 1\lambda$ and $d3 = 1.5\lambda$ of this study, the model in Figure 5 represents antenna diversity combiners. Further discussion on the differences between adaptive arrays and diversity combining is presented in [10]. The approach of maximizing the SNR at the output of the array will differ based on the configuration. First, we expand on the description of the signal in Eq. (8) to include the multipath variant and noise at the receiver. Generally, the signal model at the receiver depicted in Figure 5 characterizes the multipath propagation for channel '*l*' (the letter 'L') of the transmitted signal as a time-variant linear filter with additive noise Eq. (13).

$$x(t) = u(t) * h_l(t,\tau) + n(t)$$
$$or \qquad (13)$$
$$x(t) = \int_{-\infty}^{\infty} h_l(t,\tau)u(t-\tau)d\tau + n(t)$$

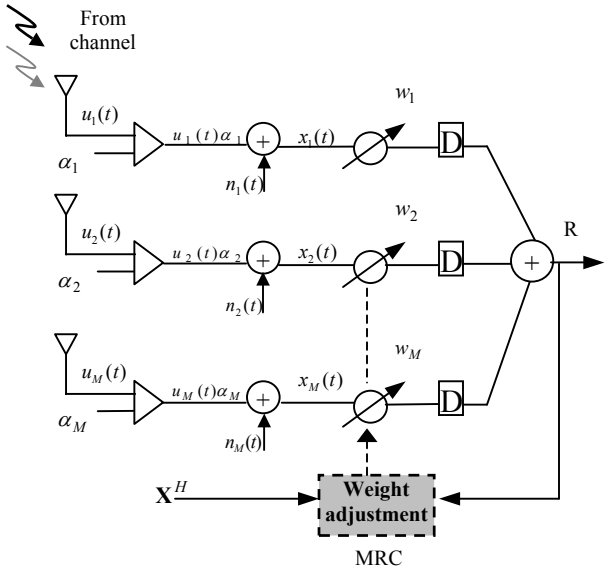

Figure 5 Combining schemes of antenna diversity vs. adaptive arrays

From Eq. (13), the time-variant impulse response $h_l(t,\tau)$ of the channel is Eq. (14)

$$h_l(t,\tau) = \sum_{l=1}^{L} A_{l,m}(t)e^{j\varphi_{l,m}(t)}\delta(t-\tau_{l,m}) \qquad (14)$$

where: each of the multipath signals comprises of an amplitude $A_{l,m}$, carrier phase shift $\varphi_{l,m}$, time delay $\tau_{l,m}$, and Doppler shift f_d, associated with the L multipaths (channels) impinging on the M antenna elements of the array.

The classical impulse response representation in Eq. (14) does not however consider the angel of arrival (AOA) of each multipath and is modified in Eq. (15) to include the AOA, which describes an accurate model of the impulse response vector at the array [14].

$$\bar{h}_l(t,\tau) = \sum_{l=1}^{L} A_{l,m}(t)e^{j\varphi_{l,m}(t)}\bar{\alpha}(\theta_{l,m}(t))\delta(t-\tau_{l,m}) \quad (15)$$

where: $\bar{\alpha}(\theta_{l,m}(t)$ is the array response vector given by

$$\alpha(\theta_l(t) = \begin{bmatrix} e^{-j\psi_{l,1}(t)} \\ e^{-j\psi_{l,2}(t)} \\ \vdots \\ e^{-j\psi_{l,M}(t)} \end{bmatrix}$$

and: $\psi_{l,m}(t) = [\kappa(\theta_l(t)]\beta$, while the first term $[\cdot]$ here represents the Cartesian coordinates of the array geometry and $\beta = \frac{2\pi}{\lambda}$.

Section 2, modeled the amplitude $A_{l,m}$ in Eq. (15) of the multipath as a Rayleigh distributed random variable and the phase shift $\varphi_{l,k}$ as a uniform distribution. Hence, to include the AOA, the received signal vector is modified to Eq. (16).

$$\bar{x}(t) = \bar{u}(t) * \bar{h}_l(t,\tau) + n(t) \qquad (16)$$

The AOAs for the 3 interelement spacing was derived using the model in Section 3 and applied in the network simulation. It should be noted that (16) includes both the direct signal and the indirect multipath signals due to the fact that we are dealing with a directive antenna array that will be pointed in the axis line to the transmitter. The weighted signal $x_m w_m$ is demodulated by the [D] block in Figure 5 on each of the branches instead of after the summer. This study does not claim to know the preference in locating the demodulator though we believe that this approach may increase the SNR per branch, although not cost-effective. This evaluation is still ongoing. The underlying objective however, is to determine optimum designs that will result in maximum SNR (without increasing the power at the transmitter. Analytically, this may be obtained by minimizing a cost-function associated with a specific algorithm to determine the optimal weight vector in Eq. (10). The criterion for algorithm selection depends largely on the intended application and channel environment. One of the most popular algorithms and that may be well suited for our application is the maximum SNR (MSNR) [12]. The MSNR requires prior knowledge of the AOA of the desired signal for which the optimum weight is obtained through minimization of its cost-function. We assume that besides the desired signal impinging on each element in the array is the additional interference/noise component *n(t)*. Then to simplify Eq. (16) we rewrite the signal *x(t)* at each antenna element as Eq. (17), where n_m is the analytical signal associated with the noise (including all the undesired signals) received by antenna *m*, and the envelope of the noise signal power is $P_{n,m} = E(n_m^* n_m)$

$$x_m(t) = s_m(t) + n_m(t) \tag{17}$$

where:

$$\begin{aligned} y_s &= \sum_{m=1}^{M} w_m s_m \\ y_n &= \sum_{m=1}^{M} w_m n_m \end{aligned} \tag{18}$$

Since the desired signal on all the elements is $\mathbf{S}_d = [s_1, s_{2,\ldots,} s_M]^T$, and the noise on all the elements is $\mathbf{N} = [n_1, n_{2,\ldots,} n_M]^T$, we may express the output *'y'* Eq. (18) at R in Figure 4, in vector notation as Eq. (19)

$$\begin{aligned} y_s &= \mathbf{W}^T \mathbf{S}_d \\ y_n &= \mathbf{W}^T \mathbf{N} \end{aligned} \tag{19}$$

The average noise power is expressed in Eq. (20)

$$\begin{aligned} &P_n = E[|y_n|^2] = E[\mathbf{w}^H \mathbf{N}\mathbf{N}^T \mathbf{w}] = \mathbf{w}^H E[\mathbf{N}\mathbf{N}^T]\mathbf{w} \\ &or \\ &P_n = \mathbf{w}^H \mathbf{R}_n \mathbf{w} \end{aligned} \tag{20}$$

where: R_n is the correlation matrix of the noise defined by $E[n(t)n(t)^H]$. The noise correlation matrix R_n for our 8-element linear array is then Eq. (21) where (*) represents convolution and the *bars* above each entry represent average.

$$R_n = \begin{bmatrix} \overline{n_1(t) * n_1(t)} & \overline{n_1(t) * n_2(t)} & \cdots & \overline{n(t) * n_8(t)} \\ \overline{n_2(t) * n_1(t)} & \overline{n_2(t) * n_2(t)} & \cdots & \overline{n_2(t) * n_8(t)} \\ \vdots & \vdots & \cdots & \vdots \\ \overline{n_8(t) * n_1(t)} & \overline{n_8(t) * n_2(t)} & \cdots & \overline{n_8(t) * n_8(t)} \end{bmatrix} \tag{21}$$

(The computation of R_n in Eq. (21) is significantly simplified by transforming the convolution in the time domain into multiplication of the individual transforms in the frequency domain). Similarly, an expression for the average signal output power may be expressed in Eq. (22)

$$P_s = \mathbf{w}^H \mathbf{R}_s \mathbf{w} \tag{22}$$

where: R_s is the correlation matrix (or the covariance matrix with zero mean) of the desired signal. The cost function then is defined as the ratio of the average noise power to the average signal (desired) power Eq. (22) [10].

$$J(w) = \frac{\mathbf{w}^H \mathbf{R}_n \mathbf{w}}{\mathbf{w}^H \mathbf{R}_s \mathbf{w}} \tag{23}$$

To minimize the cost function in Eq. (23), thus maximizing the SNR, we take the derivative of the numerator and set it to zero, i.e. we use the gradient operator ∇ on $(\mathbf{w}^H \mathbf{R}_n \mathbf{w})$ or $\nabla(\mathbf{w}^H \mathbf{R}_n \mathbf{w})$. As a sideline, it should be noted that since the diagonal elements of the noise correlation matrix in Eq. (21) are real, the matrix is Hermetian, which implies that a matrix $\mathbf{A}$ exists for which $\mathbf{A}^H \mathbf{R}_n \mathbf{A} = \mathbf{I}$ where $\mathbf{I}$ is an identity matrix. This matrix identity is essential to derive the solution for the cost-function in Eq. (23). The optimal solution to minimizing Eq. (23) is Eq. (24)[12].

$$\mathbf{R}_n^{-1} \mathbf{R}_s \mathbf{w} = \lambda_{\max} \mathbf{w} \tag{24}$$

where: $\lambda_{\max}$ is the maximum eigenvalue of the signal covariance matrix $\mathbf{R}_s$. To find the eigenvalues that satisfy Eq. (24) we expand the determinant $|R_n^{-1} R_s - \lambda I|$. The noise covariance matrix $\mathbf{R}_n = \sigma^2 \mathbf{I}$, where σ_n^2, is the noise power and $\mathbf{I}$ the identity matrix. Since $\mathbf{R}_n$ is Hermetian, it could be diagonolized to represent that all the elements have equal noise power components which are uncorrelated at the antenna elements. Adaptive arrays are by far more complex and costly to implement, though highly efficient than its counterpart with fixed weights. This does not necessarily imply that their increase in performance is cost justifiable.

The second configuration in Figure 4 that applies to the remaining interelement spacing d2 and d3 of this study represents 2 major schemes of combining in spatial diversity. Though there are many approaches to implement diversity, [7][13][15] the only schemes relevant to this study are: maximal ratio combining (MRC) with 'Weight adjustment' *(broken-line box* in Figure 4) and equal gain combining (EGC) without the 'Weight adjustment' block. As in adaptive arrays for MRC, the weights are adjusted dynamically using algorithms to minimize the error based on a feedback loop to the 'Weight adjustment' block in Figure 4, EGC on the other hand, is associated with fixed weights assignment where the 'Weight adjustment' is removed. Both MRC and EGC by virtue of combining, result in the increased average as well as the instantaneous SNRs at the receiver. For this study, the latter configuration is considered more appropriate when a deterministic approach is pursued. The combining models assumes only one transmitting antenna, M antenna elements at the receiver, and fading represented by L diversity channels carrying the same information baring signal subject to the statistics described in Section 2. Further, we assume the fading among the L diversity channels to be mutually statistically independent.

It is well known that optimum combining or OC is one of the most cost-effective spatial diversity combining techniques used to improve performance in wireless mobile communication by means of reducing the effects of fading that occurs with multipath [16]. With spatial diversity the depth of fades in Figure 1 may be reduced by summing multiple replicas of the transmitted signal that independently fade. The rationale is, that since the multipath signals experience independent fades, the probability that all of the received signals will fade below an established threshold is significantly lower than the probability that one signal among the many will fade below this threshold [15]. Suppose for example that the probability of losing communication due to a deep fade on a single branch M=1 is 10%. Then the probability of losing communications simultaneously on all M=8 branches is reduced from 0.1 to 0.1^8 i.e. the probability of loosing communication goes from 10% to $10^{-6}\%$ with 8th order diversity. In mobile ad hoc networks (as in other mobile wireless environments) the signal of interest (SOI) goes through deep fades prior to its arrival at the receiver and OC techniques may be employed to obtain significant gain in performance as demonstrated by the results of the simulation in this work.

The tradeoff of these 'combining' approaches have been the subject of many publications and continues through ongoing work in this field to explore configurations that will result in cost-effective implementations. In general, we conclude that the 'combining' approach selected is driven primarily by its intended application and cost of implementation. To obtain the best performance of the combiner the output Eq. (13) is multiplied by a complex weight value corresponding to the conjugate channel attenuation. By selecting the correct weight value, we are able to compensate for both the phase shift in the channel and loss in signal strength by scaling the amplitude of the weight assigned. For DPSK modulation, we know that the probability of error P_e as a function of the SNR/bit γ_b for an additive white Gaussian noise (AWGN) channel is

$$P_e(\gamma_b) = \frac{1}{2} e^{-\gamma_b} \tag{25}$$

where: $\gamma_b = \dfrac{E_b}{N_0}$

For a fading channel the SNR/bit is no longer $\left[\frac{E_b}{N_0}\right]$ but is equal to $\left[\alpha^2 \frac{E_b}{N_0}\right]$ where α is Rayleigh distributed. To obtain the error of probability for a DPSK fading channel, $P_e(\gamma_b)$ in Eq. (25) is averaged over the probability density function (pdf) of γ_b by evaluating the integral in Eq. (26)

$$P_e = \int_0^\infty P_f(\gamma_b) p(\gamma_b) d\gamma_b \tag{26}$$

where: $p(\gamma_b)$ is the probability density function (pdf) of $\gamma_b = \dfrac{E_b}{N_0}\alpha^2$ for the fading channel. Recognizing that α^2 is chi-square distributed (since α is a Rayleigh distributed), we express the pdf for a chi-square random variable with ν degrees of freedom Eq. (27) [9].

$$p(\chi^2) = \frac{1}{\sigma^\nu 2^{\nu/2}\Gamma(\nu/2)} (\chi^2)^{(\nu/2)-1} e^{-(\chi^2)/2\sigma^2}, \text{ for } \chi^2 \geq 0 \tag{27}$$

where: ν is the degree of freedom and $\Gamma(\cdot)$ is the Gamma function $\Gamma(a) = \int_0^\infty e^{-x} x^{a-1} dx$. Then for 2 degrees of freedom ($\nu = 2$), and by substituting $\gamma_b = \chi^2$, Eq. (27) is reduced to Eq. (28)

$$p(\gamma_b) = \frac{1}{\sigma^2 2\Gamma(1)} \gamma_b{}^0 e^{-\frac{\gamma_b}{2\sigma^2}} \tag{28}$$

where: $\Gamma(1) = 1$.

Finally, by substituting $\bar{\gamma}_b = 2\sigma^2$ in Eq. (28) the pdf of the average SNR/bit is expressed in Eq. (29).

$$p(\gamma_b) = \frac{1}{\bar{\gamma}_b} e^{-\gamma_b/\bar{\gamma}_b}, \quad \text{for } \gamma_b \geq 0 \tag{29}$$

where: the average SNR/bit in terms of α is Eq. (30)

$$\bar{\gamma}_b = \frac{E_b}{N_0} \bar{\alpha}^2 \tag{30}$$

('bars' on top denote averages).

Evaluating the integral of Eq. (26) with the appropriate substitutions Eq. (25) and Eq. (29), the probability of error $P_e(\gamma_b)$ with DPSK modulation for a fading channel is Eq. (31) [15].

$$P_e = \frac{1}{2(1+\bar{\gamma}_b)} \tag{31}$$

With diversity, the instantaneous SNR on the lth channel is $\gamma_l = \dfrac{E_b}{N_0}\alpha_l^2$ for L =1,2 … L, noting that for L=1 $\gamma_l = \gamma_b$ therefore, the instantaneous SNR for the L channels, γ_b, and the average SNR $\bar{\gamma}_c$ are expressed in Eq. (32) respectively

$$\begin{aligned} \gamma_b &= \frac{E_b}{N_0} \sum_{l=1}^{L} \alpha_l^2 \\ \bar{\gamma}_c &= \frac{E_b}{N_0} \bar{\alpha}_l^2 \end{aligned} \tag{32}$$

Substituting these new values into Eq. (27) the new pdf $p_f(\gamma_b)$ with $\nu = 2L$ degrees of freedom becomes Eq. (33).

$$p_f(\gamma_b) = \frac{1}{(L-1)!\bar{\gamma}_b^L} \gamma_b^{L-1} e^{-\frac{\gamma_b}{\bar{\gamma}_b}} \tag{33}$$

Substituting Eq. (33) into Eq. (26) and performing the integration gives the result in Eq. (34) [15] which is the error probability for DPSK when $\bar{\gamma}_c >> 1$. Figure 6 plots the results of Eq. (34), which clearly show the advantage of optimum combining as a means to mitigate the effects of fading due to multipath.

$$P_e \approx \left(\frac{1}{2\bar{\gamma}_c}\right)^L \binom{2L-1}{L} \quad (34)$$

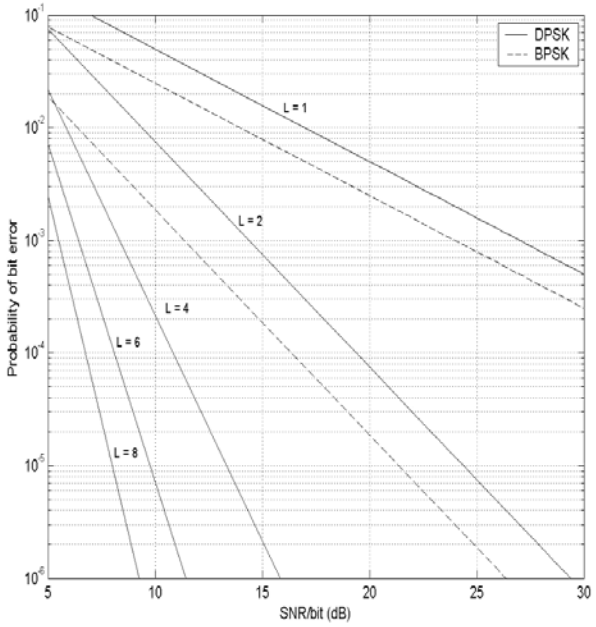

Figure 6 Performance of DPSK with M-fold combining diversity

The broken line in Figure 6 represents BPSK modulation and clearly shows that its performance is improved to that of DPSK. For large SNR, where $\bar{\gamma}_b >> 1$, the probability of error may be approximated to $P_{BPSK}(\bar{\gamma}_b) = \frac{1}{4\bar{\gamma}_b}$, while for DPSK it is $P_{DPSK}(\bar{\gamma}_b) = \frac{1}{2\bar{\gamma}_b}$. The number 4 in the denominator of the probability of error for BPSK instead of 2 for DPSK implies approximately a 3dB gain margin of BPSK over DPSK.

Employing binary PSK (BPSK) in rapidly fading channels may not produce a stable phase reference by averaging the received signal phase over many signaling intervals whereas with DPSK (differential BPSK) only two consecutive signal intervals are required which provides a robust modulation scheme for rapidly fading channels.

In principle, both the 'maximal combining ratio' and the 'equal ratio combining' spatial diversity technique (Figure 4) use complex weights to adjust the incoming signal from each antenna element which are then combined (summed) into a signal directed to the receiver's detector. The primary difference between the two techniques is that the weights associated with each of the elements in the equal ratio combining method are fixed rather than adjustable. The received signals in equal ratio combining are co-phased to provide equal gain in all directions.

5. NETWORK SIMULATION AND RESULTS

To perform the network simulation for this study we used the QualNet simulator. QualNet [6] is a discrete event high performance networking research tool, equipped with a large selection of libraries that supports channel modeling; Physical/MAC layer access protocols; routing; mobility; traffic generation for wired and wireless networks; and a built-in option that allows for configurations of antenna arrays. The radiation patterns used in the simulation (Figure 7) with the 3 variant element spacing were generated in Matlab [8]. The top row of Figure 7(a)-(c) represents the single beams that correspond to each of the variants of interelement spacing $d1 = 0.5\lambda$, $d2 = 1\lambda$, and $d3 = 1.5\lambda$ with boresight gains of 14.024, 17.013, 18.774 dB, respectively. The half power beamwidths (HPBWs – The HPBW is the angular width between the points on the main lobe that are 3dB below the boresight) for each of patterns that correspond to d1, d2, and d3 are 106°, 52°, 34°, respectively. Figure 7(d)-(f) illustrates the 8-azimuthal directional beams in increments of 45° for d1, d2, and d3. As can be seen from Figure 7(a)-(c), a narrower beamwidth is obtained as the array aperture increases (the distance between the 2 farthest elements of the array). In fact as the element spacing increased the beam became significantly more pointed and the boresight gain increased. When the distance between the antenna elements exceeded d1, the phenomena known as grating lobes occur due to under-sampling of the received radio frequency carrier that may be manifested in copies of the main lobe in unwanted directions. The Appendix illustrates the radiation pattern rotation for the d1 configuration for use with the network simulation. Actual control of the beam selection during the simulation is performed by the MAC protocol in the QualNet library.

In the network simulation, we configured an ad hoc network based on the IEEE802.11b standard [1]. We simulated a terrain of 1600x1600m with 100, 150, 200, and 250 nodes randomly distributed. Experiments were performed with the assumption that the nodes are mobile, and we used the Random Waypoint mobility algorithm (with speeds 0 to 10m/s, with 0 pause time) to implement mobility. The ad hoc on-demand vector distance (AODV) routing protocol was used in all the scenarios of the simulation. To determine the signal to interference plus noise (SINR) at the receiver, we assumed that the total noise power included thermal noise plus interference. SNR/BER lookup tables were employed to implement the differential quadrature pulse shift keying (DQPSK) modulation, which adjusts the carrier and bit timing to produce the in-phase (I) and quadrature (Q) components of the transmitted signal. The minimum threshold for the receiver to receive packets was set at -81dBm and its sensitivity at -91.0dBm. The carrier frequency used was f_c=2.4GHz with a data payload of 2Mbps. Traffic was generated using a constant bit rate (CBR) generator with a ratio of 1:5 sessions per CBR. Data transfer was 4 pps (packets/s) and each packet was set at 512 bytes in length. The results obtained from the network simulation represent an average of 5 runs with random seeds.

The distributed coordination function (DCF) of the IEEE 802.11 [1] MAC protocol was used to implement the carrier sense multiple access with the collision avoidance (CSMA/CA) algorithm. A refinement to this access method implements short control frames, request to send and clear to send (RTS/CTS), to further minimize collisions prior to data transmission. The additional overhead however, of the RTS/CTS mechanism may not be always justified [17] and as such, its use is under control of the 'dot11RTSThreshold' attribute [1]. With this attribute, nodes may be configured to use RTS/CTS either always, never, or only on frames longer than a specified length. In the simulation scenarios used for this study, the nodes are configured never to use the RTS/CTS, in order to reduce the bandwidth overhead in the network. The MAC protocol was modified accordingly to accommodate this feature.

The scenarios in the simulation are designed to represent the throughput (TP) in bits per second (bps) at the application layer. We assumed that the devices (nodes) configured to operate in an ad hoc network are retrofitted with an array. The scenarios for the network simulation comprise of the 3 variants of inter-

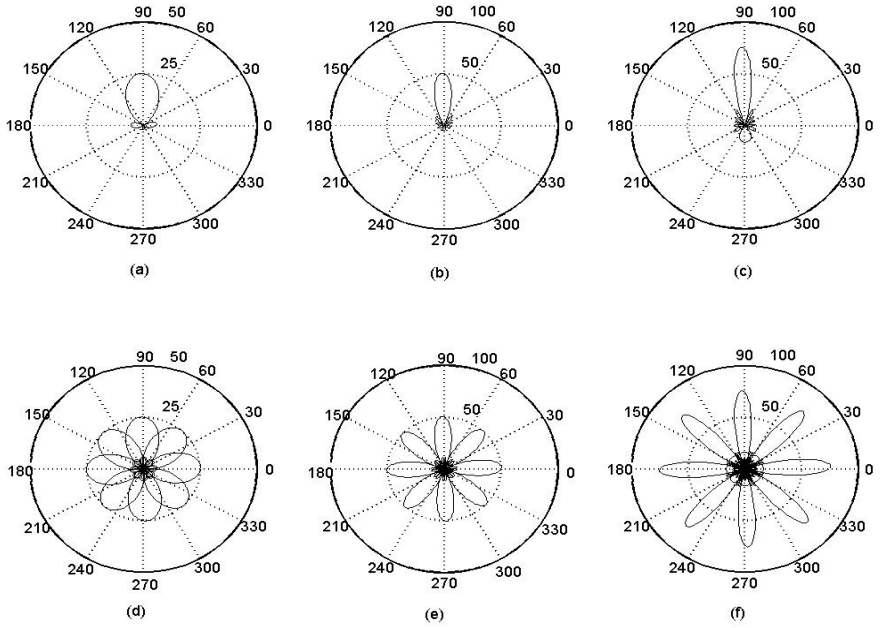

Figure 7 Radiation patterns for the 8-element UE ESLA (a) interelement spacing d1= 0.5λ (b) interelement spacing d2= 1λ (c) inter-element spacing d1= 1.5λ (d)(e)(f) respectively azimuthal increments

element spacing, $d1 = 0.5\lambda$, $d2 = 1\lambda$, and $d3 = 1.5\lambda$ (described in section 3). Thus, we empirically determine the optimum configuration that produced maximum throughput subject to the 3 interelement spacing variants. The results obtained with the antenna arrays are compared to the performance of an omnidirectional (om) antenna for both an AWGN and a fading channel.

A clear distinction is noted in the performance of the low-density scenario (where we define low-density in the range of 100-150 nodes per area = 1600x1600m), versus the high-density scenario (200-250 nodes/area). For the AWGN channel, the performance difference between the omnidirectional antenna and the arrays in the low-density network, (on the average) was negligible, less than 1%. In the high-density scenario, the performance with the arrays, on the average, was at least 18% better than with the omnidirectional antenna. Though the differences in performance in an AWGN channel are insignificant, we show the effects of the antenna inter-element spacing in a *'blow-up'* (i.e.TP coordinate 13-17 Kbps) illustrated in Figure 9a. Figure 9a shows that the array with element spacing d1 outperformed that with d2 and d3. This fact is interesting since we show that though the gain of the array with the d2 and d3 interelement spacing is greater than that with d1, yet the performance was less, which is contrary to an intuitive prediction. Employing an array is justified for channels where interference and fading significantly degrade performance to unacceptable BER levels. The results obtained from the simulation show that for the fading channel scenario (Figure 9b), the performance difference between the omnidirectional antenna and the arrays in the low-density scenario increased significantly and was computed to be within 27% on the average between the array and the omnidirectional antenna. In the high-density scenario, the performance on the average with the arrays was 60% better than that with the omnidirectional antenna. Figure 9b clearly shows that the array with the d1 element spacing again outperformed both d2 and d3 though the scanning gain was the lowest with d1. To quantify the hypothesis of improved performance through null steering, we performed a third category of simulation scenarios in which show the effects on performance with null steering (in a fading) channel as can be seen in Figure 9c. With null steering, the performance did increase for all three variants of inter-element spacing though not significantly. The relative performance improvement in the fading channel with null steering for the low-density scenario was on the average 25%, where as for high density, the improvement was 64% with respect to the performance of an omnidirectional antenna. The maximum performance in all the experiments was attained for d1.

Nulls and sidelobe effects inherent to the pattern may be viewed as detrimental to capturing the signal of interest, but nulls may also be used constructively by steering nulls in the direction of the unwanted signal. Null steering techniques are most common in radar applications and are used most effectively to reduce the effects of jammers [18] Nulling techniques are mathematically intensive and may be performed for amplitude and phase. In this study, we examined the effects of null steering empirically to mitigate the multipath and hence increase performance. As can be seen in Figure 8. The locations of the sidelobes and their magnitudes are known values.

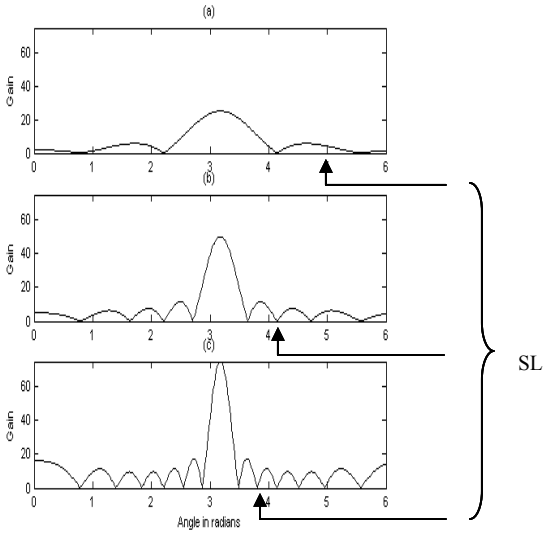

Figure 8 Radiation patterns and sidelobes (SL) Cartesian representation (a) d1 (b) d2 (c) d3)

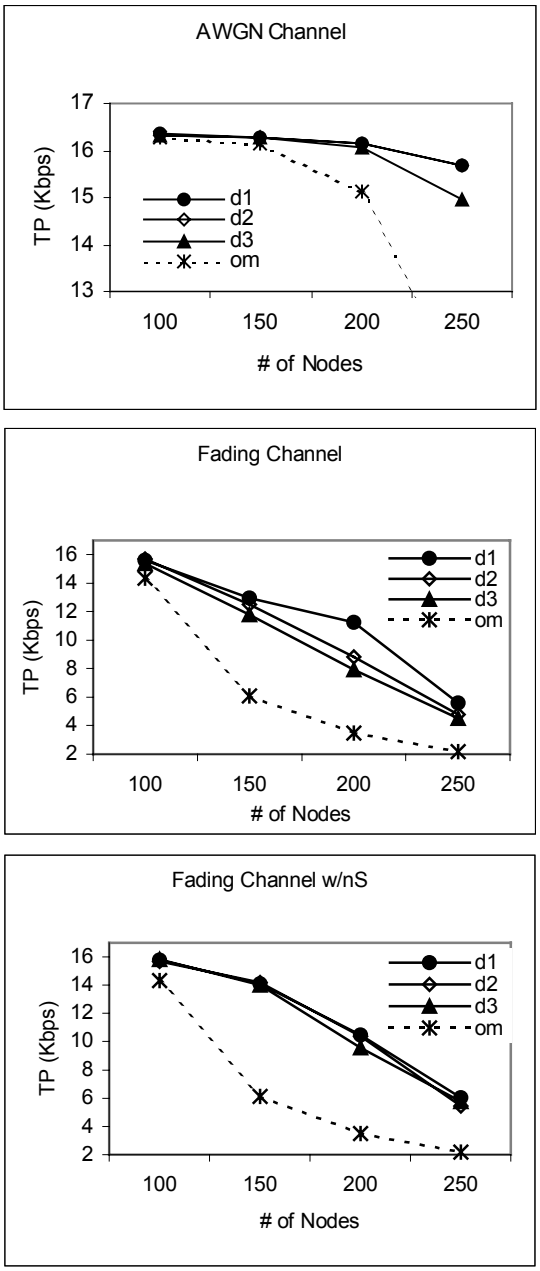

Figure 9 Throughput performance as a function of network density (a) AWGN channel (b) Fading channel (c) Null steering (ns) in a fading channel

The multipath (or interference) that arrives in the sidelobe depending on the sidelobe level (SL) is out of phase and amplified reducing the summing effect of the signal of interest arriving in the main beam. To minimize this effect steered a null in a specified direction within the angular range of the sidelobe to produce an incremental increase in the total gain. From Figure 8 it is readily seen that the effect of steering a null in the direction of the first sidelobe of Figure 8c will produce a greater differential of gain to that in Figure 8a.

We designed an optimum combiner based on co-phased received signals with constant weights and equal gain. Synthesis to reduce sidelobes deterministically in linear arrays may be obtained using Dolph-Chebyshev methods described in [11].

6. SUMMARY AND CONCLUSIONS

We show that fading channels have a detrimental effect on the performance of the network, compared to an AWGN channel, which is not realistic for mobile ad hoc networks. We quantified the fading phenomena in Section 2 by simulating rapid fading to illustrate the deep fades that occur, and discussed the need for solutions to increase the SNR at the receiver without increasing the transmitter's power. As a proposed solution, we designed an antenna array with 3 variants on the inter-element spacing to empirically determine the value of the inter-element spacing that provides the optimum combining array resulting in maximum throughput (TP) at the application layer. We performed the simulation for an AWGN and a fading channel with the 3 different patterns, each of which corresponded to a different inter-element spacing d1, d2, and d3. We examined the performance relative to each other and to that of an omnidirectional antenna in both low density and high density network configurations.

In conclusion, the array consistently performed better than the omnidirectional antenna in all cases. Interestingly, d1 performed the best though the gain of the array was the lowest, and d3 with the largest aperture, (corresponding to the array with the most gain in its boresight), consistently produced the lowest results. Intuitively, one would expect the results to be contrary to those obtained since it is natural to assume that the antenna array with the maximum gain (largest aperture) will produce the best results (BER), which indeed is the case in a point-to-point scenario. However, the dynamics of the network together with the steering mechanisms controlled by the MAC with the prescribed access mechanism of the ad hoc network, combine into multiple dimensionality effects that affect the network performance in a somewhat unpredictable manner.

It is easy to see from Figure 7f that though the main beams are pointed and have a larger gain, the narrow HPBW has a detrimental effect in the network since the signal may arrive between the beams where the energy is insufficient to meet the sensitivity threshold of the receiver. In contrast, the beams in Figure 7d have a large HPBW of a 102^{o} where the overlap of the beam is significantly apparent and compensates for the full 360^{o} coverage. In fact, it is readily seen in Figure 7d that with the d1 array, the degradation effect in mobility scenarios regardless of the location of the node would be significantly less than with the d2 and d3 arrays in Figure 7e, f respectively.

To further improve performance, we investigated the performance with null steering to mitigate multipath and interference. The results were better but not by far. The differential of performance increase as a result of the null steering was more apparent with d3, Figure 8c rather than with d1, Figure 8a. This is consistent with expectations since the sidelobe level for d3 was greater than that for d1 (as the gain of the boresight increased so did sidelobe level increase). With null steering, the differential of improvement between the scenarios with and without null steering was 9% for d3, 5% for d2 and less than 1% for d1 which is evident in Figure 8.

In future work we plan to exploit the effects of coding introduced by spread spectrum [16] and angle sensitivity of adaptive arrays to enhance the process of maximizing the SNR at the receiver in the off-angle and off-time response of undesirable indirect multipath.

APPENDIX

Figure A1 illustrates the rotational positions for the 8-element UA ESLA designed with Matlab for use in the network simulation. The radiation pattern in Figure A1 was derived using d1 interelement spacing. The first beam (aligned on the horizontal axis, pointing to the right) is of broadside type that is rotated in increments of 45^o clockwise.

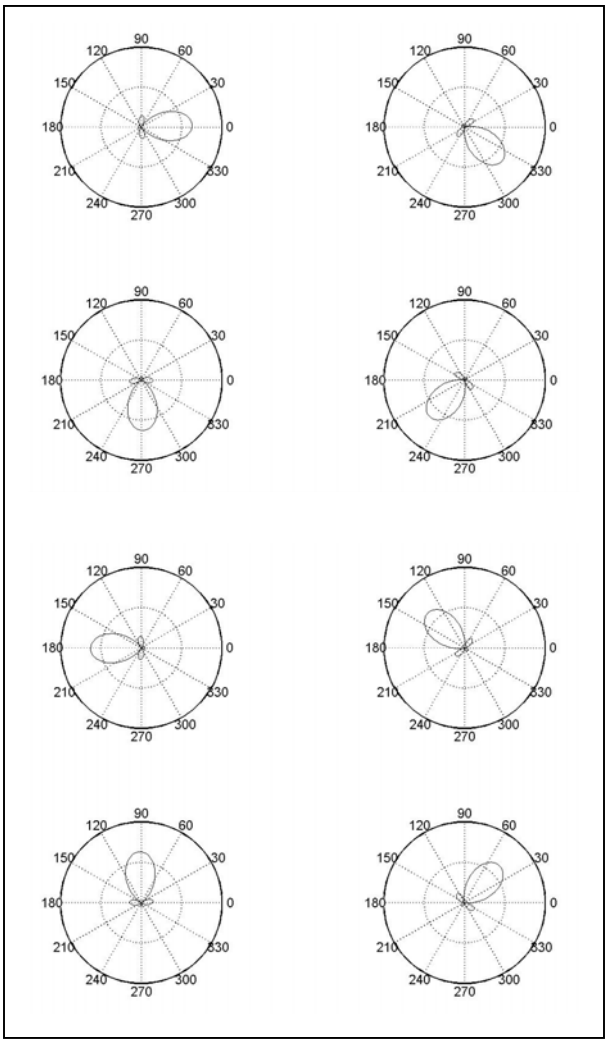

Figure A1 Radiation pattern rotation

The directivity *D* of a broadside array for the isotropic elements used in this work is approximated by $D \approx 2\frac{Md}{\lambda}$ (where M is the number of elements in the array). *Md* is usually referred to as the array length. Hence, it is easy to see that the directivity will increase with either/or the number of elements or with element interspacing. (This is clearly illustrated in Figure 7). Directivity is defined as the "Ratio of power density in the direction of the pattern maximum to the average power density at the same distance from the antenna" [11]. Gain is merely the directivity reduced by the losses of the antenna. For isotropic antenna elements, we assume that there are no losses. Hence, gain is the same as directivity in this study. All the beams have fixed gain (weights are fixed not adaptive). Each radiation pattern is represented by a 3x8x360 i.e. table that corresponds to the beam index number, the gain (in dB) tabulated in 360 increments per beam position. Hence, the final matrix for the simulation is 3 columns and 2880 rows per radiation pattern.

REFERENCES

[1] Institute of Electrical and Electronics Engineers, Inc., "*IEEE Standard 802.11b: Supplement to IEEE Standard for Information Technology. Telecommunication and information exchange between systems, Local and metropolitan area networks, Specific requirement: Part 11:Wireless LAN Medium Access Control (MAC) and Physical Layer (PHY) Specifications: Higher-Speed Physical Layer Extension in the 2.4 GHz Band,"* IEEE, Inc., New York, NY, 2000.

[2] N.C. Karmakar, and M.E. Bialkowski, "A Beam-Forming Network for Circular Switched-Beam Phased Array Antenna", *IEEE Microwave and Wireless Components Letters*, vol. 11, no. 1, pp. 7-9, Jan. 2001.

[3] Y-B. Ko, V. Shankarkumar, and N.H. Vaidyn, "Medium Access Control Protocols using Directional Antennas in Ad Hoc Networks", IEEE INFOCOM, pp 13-21, May 2000.

[4] A. Nasipuri, S. Ye, J.You, and R.E. Hiromoto, "A MAC Protocol for Mobile Ad Hoc Networks Using Directional Antennas", Wireless Communications and Networking Conference, >2000. WCNC. 2000. IEEE, vol.3, pp. 1214-1219, 2000.

[5] R. Ramanathan, "On the performance of Ad Hoc Networks with Beamforming Antennas", Proceedings of The 2001 ACM International Symposium on Mobile Ad Hoc Networking & Computing, Oct. 4-5, 2001, Long Beach, CA, pp. 95-105, 2001.

[6] *QualNet Simulator & User's Manual*, Scalable Network Technologies, Inc., Los Angeles, CA, 2002.

[7] T. S. Rappaport, *Wireless Communications Principles and Practice*, Upper Saddle River, NJ, Prentice Hall PTR, 1996

[8] *Using Matlab*, Version 6, Natick, MA, The MathWork, Inc., 2000.

[9] J. L. Devore, *Probability and Statistics for Engineering and the Sciences*, 6th Edition, US, Thomson Brooks/Cole, 2004.

[10] J.C. Liberty, Jr., and T.S. Rappaport, *Smart Antennas for Wireless Communications: IS-95 and Third Generation CDMA Applications*, Upper Saddle River, NJ, Prentice Hall PTR, 1999.

[11] W. L. Stutzman, and G. A. Thiele, *Antenna Theory and Design*, Second Edition, New York, NY: John Wiley & Sons, Inc., 1998.

[12] R.A. Monzingo, and T.W. Miller, *Introduction to Adaptive Arrays*, New York, NY, John Wiley & Sons, 1980.

[13] R. L. Peterson, R.E. Ziemer, and D.E. Borth, Introduction *to Spread Spectrum Communications*, Englewood Cliffs N.J., Prentice Hall, 1995.

[14] R. B. Ertel, P. Cardieri, K. W. Sowerby, T.S. Rappaport, and J. H. Reed, "Overview of Spatial Channel Models for Antenna Array Communication Systems," *IEEE Personal Communications,* Feb. 1998, pp. 10-22.

[15] J. G. Proakis, *Digital Communications*, 4th Edition, New York, NY, McGraw-Hill, Inc., 2001.

[16] S. Furman, and M. Gerla, "The Design of a Spatial Diversity Model to Mitigate Narrowband and Broadband Interference in DSSS Ad Hoc Networks," *IEEE International Conference on Communications*, May 2003 .

[17] M. Gerla, and F. Talucci, "MACA-BI (MACA By Invitation) A Wireless MAC Protocol for High Speed ad hoc Networking," *Universal Personal Communication Records*, *IEEE 6th International Conference*, Vol. 2, pp. 913-917, Oct. 12-16, 1997.

[18] D. E. Hammers, and R. H. Fletcher "Radar Systems, A System Theoretic Approach," *24th Midwest Symposium on Circuits and Systems,* pp. 588-597, Jun. 29-30, 1981.